A new sea surface temperature proxy based on bacterial 3-hydroxy fatty acids

Yang, Yi; Wang, Canfa; Bendle, James A.; Yu, Xiaoguo; Gao, Chao; Lü, Xiaoxia; Ruan, Xiaoyan; Wang, Ruicheng; Xie, Shucheng

DOI:
10.1016/j.orggeochem.2020.103975

Journal Pre-proofs

A new sea surface temperature proxy based on bacterial 3-hydroxy fatty acids

Yi Yang, Canfa Wang, James A. Bendle, Xiaoguo Yu, Chao Gao, Xiaoxia Lü, Xiaoyan Ruan, Ruicheng Wang, Shucheng Xie

PII: S0146-6380(20)30010-3
DOI: https://doi.org/10.1016/j.orggeochem.2020.103975
Reference: OG 103975

To appear in: *Organic Geochemistry*

Received Date: 28 May 2019
Revised Date: 5 January 2020
Accepted Date: 8 January 2020

Please cite this article as: Yang, Y., Wang, C., Bendle, J.A., Yu, X., Gao, C., Lü, X., Ruan, X., Wang, R., Xie, S., A new sea surface temperature proxy based on bacterial 3-hydroxy fatty acids, *Organic Geochemistry* (2020), doi: https://doi.org/10.1016/j.orggeochem.2020.103975

A new sea surface temperature proxy based on bacterial 3-hydroxy fatty acids

Yi Yang[a], Canfa Wang[a,*], James A. Bendle[b], Xiaoguo Yu[c, d], Chao Gao[e], Xiaoxia Lü[f], Xiaoyan Ruan[g], Ruicheng Wang[e], Shucheng Xie[a]

[a] *State Key Laboratory of Biogeology and Environmental Geology, Hubei Key Laboratory of Critical Zone Evolution, School of Earth Sciences, China University of Geosciences, Wuhan, 430074, China*

[b] *School of Geography, Earth and Environmental Sciences, University of Birmingham, Birmingham, B15 2TT, UK*

[c] *Key Laboratory of Submarine Geosciences, State Oceanic Administration, Hangzhou 310012, China*

[d] *Second Institute of Oceanography, Ministry of Natural Resources, Hangzhou 310012, China*

[e] *State Key Laboratory of Biogeology and Environmental Geology, China University of Geosciences, Wuhan, 430074, China.*

[f] *College of Marine Science and Technology, China University of Geosciences, Wuhan 430074, China*

[g] *Key Laboratory of Tectonics and Petroleum Resources of Ministry of Education, China University of Geosciences, Wuhan, 430074, China*

*Corresponding author. Tel: +86 2767883452 Fax: +86 2767883456 E-mail address: wangcf@cug.edu.cn (C. Wang).

ABSTRACT

3-Hydroxy fatty acids (3-OH-FAs), derived from Gram-negative bacterial outer membranes, have received recent attention for their potential as new terrestrial pH and temperature proxies for palaeoclimate studies. However, it is not known whether 3-OH-FAs based proxies can be developed and applied to the marine environment. Here we analyze 3-OH-FAs from a latitudinal transect of marine surface sediments from the North Pacific Ocean (12 °N to 61 °N with a mean annual sea surface temperature (SST) range of 28.1 °C to 1.3 °C). The results show that distributions of 3-OH-FAs in marine sediments yield overall higher abundances of *anteiso* 3-OH-FA homologues compared to soils. Furthermore, 16S rRNA gene sequencing of the marine sediments and soils shows the Gram-negative bacterial community is dominated by Proteobacteria (ca. 94%) at the phylum level. In contrast, in regional soils the Gram-negative bacterial community is more diverse with significant contributions from Proteobacteria (ca. 50%), Acidobacteria (ca. 24%), Verrucomicrobia (6%), Bacteroidetes (6%) and other phyla. These distinct genomic and molecular differences suggest distinctly different aggregate compositions of bacteria that produce 3-OH-FA in the marine realm vs soils. Moreover, we find that the ratio of *anteiso* to *normal* C_{13} 3-OH-FA (RAN_{13}) measured in surface sediments is highly correlated with mean annual SST throughout the temperature transect (1.3–28.1 °C). When applied to a short sediment core from the East China Sea, the SST changes reconstructed by the RAN_{13} proxy are comparable to instrumental SST data. These findings demonstrate that RAN_{13} and potentially other, so far undiscovered, proxies based on 3-OH-FAs have potential for environmental and palaeoclimate applications in marine environments.

Keywords: 3-Hydroxy fatty acids; Marine sediment; Soil; Sea surface temperature (SST); Temperature proxy; Palaeoclimate; Pacific Ocean.

1. Introduction

To better understand the climate system and to provide a palaeoclimatic context for predictions of future rates of climate change, a wide range of environmental information from both terrestrial and marine realms is required from palaeoclimate archives. The determination of past sea surface temperatures (SSTs) is critical as SSTs are coupled to general atmospheric circulation. SSTs are also one of the dominant controls on microbial community composition and phytoplankton distribution in marine environments and thus also higher tropic levels. During the past three decades, several proxies based on lipid biomarkers have been proposed for reconstructing SST, inter alia: the $U^{K'}_{37}$ proxy based on long-chain alkenones (C_{37}, C_{38} and C_{39}) (Brassell et al., 1986; Conte et al., 2006; Rosell-Melé and Prahl, 2013; Tierney and Tingley, 2018), TEX_{86} (TetraEther indeX of tetraethers consisting of 86 carbon atoms) based on isoprenoid glycerol dialkyl glycerol tetraethers (isoGDGTs) (Schouten et al., 2002; Kim et al., 2008, 2010), and the Long chain Diol Index (LDI) based on long chain diols compounds (Rampen et al., 2012). These existing palaeothermometers have been widely applied to reconstruct SSTs at various spatial and temporal scales through the Holocene (Moossen et al., 2015), Quaternary (Naafs et al., 2012; Lopes dos Santos et al., 2013) and deeper time in the Cenozoic and Mesozoic (Herbert and Schuffert, 1998; Bijl et al., 2013; Inglis et al., 2015; Herbert et al., 2016; Robinson et al., 2017; de Bar et al., 2019).

However, environmental factors other than temperature (e.g., nutrients, seasonality, export production depth, salinity, pH and biological source) may influence the above biomarker proxies in certain contexts, especially in marginal basins and at warm or cold extremes of the temperature calibrations (Kim et al., 2008, 2010; Trommer et al., 2009). The $U_{37}^{K'}$ proxy, derived from haptophytes has been widely applied to sediments spanning the last 3.5 Ma (Herbert et al., 2010). Generally, alkenones reflect mean annual SSTs except in regions with a shortened season for phytoplankton growth (Sikes et al., 2005; Conte et al., 2006; Versteegh et al., 2007; Yamamoto et al., 2007; Rosell-Melé and Prahl, 2013; Moossen et al., 2015; Tierney and Tingley, 2018). Factors that could bias $U_{37}^{K'}$ records away from mean annual SSTs include nutrient and light limitation (Herbert, 2003), changes in the dominant species responsible for alkenone production (Volkman et al., 1995), seasonality (Sikes et al., 1997; Moossen et al., 2015), salinity (Fujine et al., 2006) and nutrient dynamics (Epstein et al., 1998; Eltgroth et al., 2005).

TEX_{86} is broadly correlated to SST in extensive global core top calibrations (Kim et al., 2008, 2010). However, there is evidence that TEX_{86}-based temperature estimates can be influenced by seasonality (Herfort et al., 2006), non-thermal effects such as water depth (Wei et al., 2011; Taylor et al., 2013; Hernández-Sánchez et al., 2014; Seki et al., 2014; Kim et al., 2015, 2016; Villanueva et al., 2015;), in situ GDGT production in sediments (Lipp and Hinrichs, 2009; Zhang et al., 2011), sediment diagenesis (Schouten et al., 2004), and catchment-derived isoGDGTs from Thaumarchaeota living in soils (Weijers et al., 2006). Recent culture studies (Elling et al., 2015) have found that there is not a common linear TEX_{86} response to growth temperature in cultivated strains of Thaumarchaeota. Eley et al. (2019) recently applied machine-learning tools

(e.g., Gaussian Process Emulators) to the isoGDGT global calibration dataset and found a strong, underlying temperature-dependence, but also highlighted how fossil GDGT distribution patterns differed significantly from the modern especially in the Eocene and Cretaceous. Finally, the LDI index, derived from diols produced by microalgae, has been applied to reconstruct SSTs throughout the Quaternary (Naafs et al., 2012; Rodrigo-Gámiz et al., 2014). However, it appears to be of limited application to marginal oceans where river input is predominant (Rampen et al., 2012; de Bar et al., 2016). In addition, reconstruction of SSTs with multiple proxies in southeastern Australia for the last ~135 ka revealed that the LDI-inferred temperatures are close to the temperature of the warmest month, and TEX_{86}^{H} to austral winter month SST and $U_{37}^{K'}$ to the mean annual SST (Lopes dos Santos et al., 2013). Overall, the existing temperature proxies all come with their own strengths, but also with numerous caveats, which makes accurate temperature estimation a continuing challenge for marine sediments.

Gram-negative bacterially derived 3-hydroxy fatty acids (3-OH-FAs) are commonly found in marine and terrestrial environments, including in marine particulate organic matter and sediments (Wakeham, 1999, 2003; Wang et al., 2016), lake sediments (Wang et al., 2016), speleothems (Wang et al., 2012, 2018), soils (Zelles et al., 1995; Wang et al., 2016; Yang et al., 2016) and fresh snow (Tyagi et al., 2015). 3-OH-FAs with carbon numbers from C_{10} to C_{18} are mainly derived directly from the lipid A component of lipopolysaccharide (LPS), the outer membrane of Gram-negative bacteria (Cranwell, 1981; Raetz et al., 2007). Laboratory culture experiments show that different Gram-negative genera and species produce differing 3-OH-FAs compositions (Oyaizu and Komagata, 1983; Goossens et al., 1986; Hedrick et al., 2009; Wang et al.,

2018). Since both membrane lipid structure (Denich et al., 2003) and microbial community composition (Bahram et al., 2018) respond to environmental changes, 3-OH-FA homologs in environmental samples may encode information on environmental parameters.

However, these biomarkers have been largely overlooked for palaeoclimate applications until recently (Wang et al., 2016, 2018; Huguet et al., 2019). Wang et al. (2016) proposed novel terrestrial proxies based on 3-OH-FAs as independent pH and temperature proxies based on altitudinal transects of soil samples from central China. Two temperature proxies, RAN_{15} (the ratio of *anteiso* to *normal* C_{15} 3-OH-FA) and RAN_{17} (the ratio of *anteiso* to *normal* C_{17} 3-OH-FA), show linear relationships with mean annual air temperature (MAAT). Furthermore, a number of 3-OH-FA indices, including the Branching Ratio and the negative logarithm of the Branching Ratio (RIAN) – which quantify the proportion of *iso* and *anteiso* to the *normal* 3-OH-FAs – were well correlated with soil pH, and show a linear correlation with the cyclization ratio of branched bacterial GDGTs (CBT – a proxy for pH; Wang et al., 2016) in the same samples. These proxies were recently applied to the HS4 stalagmite in central China (Wang et al., 2018), representing the first palaeoclimate application of 3-OH-FAs and also, more generally, the first independent, biomarker-based, temperature and hydrological reconstructions from a speleothem.

Thus 3-OH-FAs show potential for terrestrial palaeoclimate reconstruction. However, whether the application of the existing 3-OH-FA based temperature and pH proxies is feasible in marine systems is still unknown. Gram-negative bacteria are the dominant prokaryotes in the ocean (Giovannoni, 2000) and 3-OH-FAs are found in detectable abundance in marine particulate matter and sediments (Kawamura et al.,

1987; Wakeham, 1999, 2003). Therefore, it is reasonable to consider the possibility of 3-OH-FA based applications in the marine environment. In this study, we investigate 3-OH-FA distributions along a marine latitudinal surface sediment transect. We utilize 16S rRNA analyses to place constraints on the biological source of 3-OH-FAs in the marine sediments. Finally, we test existing terrestrial 3-OH-FA based proxies in marine sediments and propose a novel 3-OH-FA based SST proxy, RAN_{13}, specifically for use in marine environments.

2. Sampling and methods

2.1. Sampling

We collected 45 marine surface sediments across a latitudinal range from 12 °N to 61 °N. The transect encompasses seven different marginal seas (South China Sea, East China Sea, Yellow Sea, Bohai Sea, Japan Sea/East Sea, Okhotsk Sea, and Bering Sea; Fig. 1) and spans a diverse range of environmental settings from the tropics to regions with seasonal sea-ice cover. Accordingly, the transect covers a wide range of mean sea surface temperature (SST) from 1.3 °C to 28.1 °C. Sub-samples for geochemical analyses were extracted from the surface 0–5 cm of box cores, collected from water depths ranging from 7 m to 3960 m. In addition, a short box core B3 (29 cm; 27°19.056'N, 121°39.246' E; Fig. 1) was collected in July 2017 from the East China Sea. The core surface was well preserved upon collection, and the upper water above the sediment surface in the box corer was clear. After syphoning out the overlying water, a core barrel was pushed into the box to remove a sub-core. Sediment in the sub-core was extruded and sectioned at 1 cm intervals. Each sample was collected and wrapped in pre-cleaned foil and sealed in a jar. In addition, soil samples (n = 3) and

marine sediments (n = 3) for genetic analysis were collected from Mt. Yujia (Wuhan) and the South China Sea, respectively. All the samples were frozen at –20 °C before further analysis.

For each sampling site, mean satellite SSTs were calculated using the recent 30-year annual average (1981–2011) SSTs obtained from the World Ocean Atlas 2018 (WOA18), provided by the National Oceanographic Data Center, which computes SST globally with a 1° spatial resolution. We also obtained instrumental mean annual and seasonal SSTs since 1950 from NOAA for comparison with the B3 core from the East China Sea (https://www.esrl.noaa.gov/psd/). To further explore environmental influences on the distribution of 3-OH-FAs, we processed other parameters such as water salinity, pH, nitrate, phosphate and silicate concentration over a period of 10 years (from January 2008 to May 2018), obtained from the NOAA National Centers for Environmental information with a 1° spatial resolution (Supplementary Data). All the surface temperature and nutrient concentrations were downloaded from the website (https://www.nodc.noaa.gov/OC5/woa18/woa18data.html).

2.2. Sediment dating

The ^{210}Pb method was used for determining the chronology of the box core. ^{210}Pb measurements were performed using ORTEC HPGe detectors (GEM, Lo-Ax and GMX) at the Nanjing Institute of Geography and Limnology. International standard reference materials IAEA-133A, IAEA-327, and IAEA-375 were used to determine the energy, efficiency, and mass calibration of each detector. Constant ^{210}Pb activities in the lower portion of the core are assumed to represent the 'supported' ^{210}Pb activity, and this

value was subtracted from total activity to yield excess ^{210}Pb activity ($^{210}Pb_{ex}$). The accumulation rate was calculated using a constant initial concentration (CIC) model (Oldfield et al., 1978).

2.3. Organic geochemistry

2.3.1. 3-OH-FAs analysis

Marine surface sediment samples (n = 45) were extracted using an optimized acid digestion method (Wang et al., 2012). Specifically, 10 g of each sample was digested using 3 M HCl at 130 °C for 3 h. The internal standard 3-hydroxytetradecanoic acid-2,2,3,4,4-d5 (DL-3-hydroxymyristic acid) was added to each sample before digestion. After cooling, the solutions were extracted by dichloromethane (DCM) 5 times, to obtain the total lipid extract (TLE). The TLE was concentrated to 1–2 mL using a rotary evaporator (Buchi R210, Switzerland) with a water heating bath at 38 °C and then dried under a gentle N_2 flow. TLEs were methylated at 70 °C for 1.5 h by adding 2 mL BF_3-MeOH solution. The fatty acid methyl esters (FAMEs) were extracted using *n*-hexane, and separated into non-OH-FAMEs and OH-FAMEs by activated silica gel column chromatography by eluting with a mixture of solvents (*n*-hexane:ethyl acetate (98:2, v/v)) and 100% ethyl acetate, respectively (Jenske and Vetter, 2008). The OH-FAMEs were further derivatized with N,O-*bis*-(trimethylsilyl)trifluoroacetamide (BSTFA) at 70 °C for 1.5 h before analysis by GC–MS within 24 h. Care was taken at all stages, when concentrating solvent fractions, to use a gentle N_2 flow to minimize any potential loss of lower molecular weight fatty acids.

The 3-OH-FA fraction was analyzed with an Agilent 7890A gas chromatograph and a 5975C mass spectrometer equipped with a DB-5MS fused silica capillary column

(60 m × 0.25 mm id.; 0.25 μm film thickness). The GC oven temperature was programmed from 70 to 200 °C at 10 °C min^{-1}, then to 310 °C at 3 °C min^{-1}, held at 310 °C for 47 min. Helium (99.999% pure) was used as the carrier gas and the gas flow was 1.0 mL min^{-1}. The ionization energy of the mass spectrometer was set at 70 eV. The 3-OH-FAs were identified based on their mass spectra and relative retention times. The 3-OH-FAME TMSi ethers show diagnostic fragment ions, *m*/*z* 175 $([CH_3]_3SiO{=}CHCH_2CO_2CH_3)^+$, due to the cleavage between C3 and C4, and $[M–15]^+$ (base peak) which results from a loss of a CH_3 group (Eglinton and Hamilton, 1967; Wang et al., 2016). The DL-3-hydroxymyristic acid shows the diagnostic fragment ion *m*/*z* 178 $([CH_3]_3SiO{=}CDCD_2CO_2CH_3)^+$, containing three deuterium atoms in the fragment.

2.3.2. isoGDGTs analysis

Surface sediment isoGDGT data had been published for four of the South China Sea samples in Yang et al. (2018) and 12 of the East China Sea samples in Lü et al. (2014). We measured isoGDGTs in 15 additional surface sediment samples and for the B3 samples using the same method as Lü et al. (2014). Briefly, dry samples were extracted using dichloromethane (DCM) and MeOH (9:1, v/v) using ultrasonication for 15 min (×4). The supernatants from each extraction were combined and concentrated, using rotary evaporation to 1–2 mL of TLE. Then the TLE was transferred using DCM to 8 mL vials and dried under N_2. TLEs were separated over an activated silica and anhydrous sodium sulfate column into nonpolar and polar fractions, using hexane and MeOH, respectively. The polar fraction (containing GDGTs) was saponified with 0.5 M KOH in MeOH at 70 °C for 2 h, then extracted (×5) with *n*-hexane. The polar fraction

was concentrated to 1–2 mL under N_2 and passed through a 0.45 μm PTFE filter to remove particulate matter.

The polar fraction was re-dissolved in 300 μL *n*-hexane/isopropanol (99:1, v/v) and spiked with a known amount of internal standard, C_{46} GTGT (Huguet et al., 2006). GDGTs were analyzed using a high-performance liquid chromatography atmospheric pressure chemical ionization-mass spectrometer (HPLC–MS; Agilent 1200 series, triple quadrupole mass spectrometer) equipped with Masshunter qualitative software and an auto-injector. Separation of GDGTs was achieved with an Alltech Prevail Cyano Column (150 × 2.1 mm, 3 μm), the elution gradient and the MS conditions followed Schouten et al. (2007). The isocratic elution was used for the first 5 min with 90% A and 10% B, where A = *n*-hexane and B = *n*-hexane/isopropanol (9:1, v/v). The following gradient was then used: 90:10 A/B to 82:18 A/B from 5 to 45 min. Between samples, the column was washed with 100% B for 10 min and then equilibrated with 90:10 A/B, with a constant flow rate of 0.2 mL/min. Single ion monitoring (SIM) was used, and compound quantification was performed by peak area integration of $[M+H]^+$ in the extracted ion chromatogram, targeting *m*/*z* 1302, 1300, 1298, 1296, 1292 (common isoGDGT protonated molecular ions). The final results can only be considered as semi-quantitative as we did not determine the relative response factors between individual GDGTs and the internal standard.

2.4. DNA extraction and 16S rRNA gene sequencing

2.4.1. DNA extraction

The surface of the sediment samples was discarded to avoid contamination. Then, 0.5 g of each sample was subjected to DNA extraction using the CTAB/SDS method

(Niu et al., 2008). DNA concentration and purity were checked using a Nanodrop 2000 spectrophotometer (Thermo Scientific, Delaware, USA) and stored at –20 °C for further analysis.

2.4.2. 16S rRNA gene sequencing

Total genome DNA was extracted using the CTAB/SDS method (Niu et al., 2008). The 16S rRNA target genes for the V4 distinct regions were amplified using the primer set 515F (5'-GTGCCAGCMGCCGCGGTAA-3') and 806R (5'-GGACTACVSGGGTATCTAAT-3') for targeting DNA fragments longer than 300 base pairs (Bergmann et al., 2011). DNA samples were processed by Beijing Novegene Bioinformatics Technology Co. Ltd. (Beijing, China) for amplicon sequencing using the Illumina MiSeq platform with the HiSeq PE250 system (Illumina, California, USA). The forward primers contain a 6-bp error-correcting barcode unique to each sample. The DNA was amplified following the protocol described previously (Caporaso et al., 2011).

2.4.3. Bioinformatics and statistical analysis

For 16S rRNA gene sequencing data, pairs of reads from the original DNA fragments were merged with fast length adjustment of short reads (FLASH) (Magoc and Salzberg, 2011). Single-end reads were assigned to samples based on their unique barcode and truncated by cutting off the barcode and primer sequence. Quantitative Insights Into Microbial Ecology (QIIME) and UPARSE pipeline (Caporaso et al., 2010) were used to filter the reads and to extract the operational taxonomic units (OTUs) with > 97% similarity, respectively. Then, for each OTU, a representative sequence was

selected using Ribosomal Database Project (RDP) classifier to assign taxonomic composition (Wang et al., 2007; Cole et al., 2009). OTU abundance information was normalized using a standard with a sequence number corresponding to the sample with the least sequences. Statistical analysis was based on the OUT taxonomic composition and OUT abundance. We use localized BugBase software to predict bacterially relevant phenotypes based on ribosomal 16S rRNA datasets. BugBase leverages pre-existing database, annotation and framework data, along with manual curation to provide the user with microbial phenotype predication at the organism level, including Gram staining, oxygen tolerance, biofilm formation, pathogenicity, mobile element content and oxidative stress tolerance (Ward et al., 2017).

2.5. Statistical analysis

Statistical analyses were performed to examine the relationship between 3-OH-FA based indices and environmental parameters in both our new marine and previously published soil datasets (Wang et al., 2016, 2018; Huguet et al., 2019). Principal component analysis (PCA) was performed on the fractional abundance of 3-OH-FA homologues to provide a general view of the variability within the distribution of 3-OH-FAs between soils and marine sediments. The relationships between 3-OH-FAs and environmental factors, such as SST, water depth, pH, salinity, and nutrient conditions, were assessed by applying redundancy analysis (RDA). All statistical analyses were conducted using the software Canoco 5.0.

2.6. Proxy calculations

With the exception of our newly proposed RAN_{13} index, all 3-OH-FA based indices

were calculated following Wang et al. (2016):

$RAN_{15} = a\text{-}C_{15} / n\text{-}C_{15}$ 3-OH-FA (1)

$RAN_{17} = a\text{-}C_{17} / n\text{-}C_{17}$ 3-OH-FA (2)

$RIN = I/N$ (3)

Branching Ratio $= (I + A)/N$ (4)

$RIAN = -\log [(I + A)/N]$ (5)

Branched Index $= (I + A)/(I + A + N)$ (6)

Where *a* and *n* represent *anteiso* and *normal* 3-OH-FA, *I* represents the sum of all the *iso* 3-OH-FAs, *A* represents the sum of all the *anteiso* 3-OH-FAs, and *N* represents the sum of all the *normal* 3-OH-FAs.

isoGDGT-based indices and inferred SST were calculated following Kim et al. (2008, 2010).

$TEX_{86} = (GDGT\text{-}2 + GDGT\text{-}3 + Cren')/(GDGT\text{-}1 + GDGT\text{-}2 + GDGT\text{-}3 + Cren')$ (7)

$TEX_{86}^{H} = \log (TEX_{86})$ (8)

$TEX_{86}^{L} = \log((GDGT\text{-}2)/(GDGT\text{-}1 + GDGT\text{-}2 + GDGT\text{-}3))$ (9)

$SST = 56.2 \times TEX_{86} - 10.78$ $(n = 233, R^2 = 0.935)$ (10)

$SST = 68.4 \times TEX_{86}^{H} + 38.6$ $(n = 255, R^2 = 0.87)$ (11)

$SST = 67.5 \times TEX_{86}^{L} + 46.9$ $(n = 396, R^2 = 0.86)$ (12)

3. Results

3.1. Sediment chronology

The $^{210}Pb_{ex}$ activity profiles for the B3 core collected from the ECS are shown in

Fig. 2. The ^{210}Pb ages indicate that B3 has been accumulating sediments since ca. 1959 with a mean accumulation rate of 0.49 cm yr^{-1}. The accumulation rates agree well with reported data from the adjacent ECS shelf (Chen et al., 2014; Xu et al., 2015; Lin et al., 2016). The B3 core has accumulation rates slightly lower than observed in cores DZ18 and DZ41 collected from the Zhejiang-Fujian Coastal mud area (Chen et al., 2017), which is consistent with B3 occupying a location in deeper water that is relatively farther from the Yangtze River mouth (and thus fluvial inputs).

3.2. The concentration and distribution of 3-OH-FAs in marine sediments and core B3

3-OH-FA homologues, including *normal*, *iso* and *anteiso* 3-OH-FAs, were detected in all marine surface sediments (Fig. 3). The total concentrations of 3-OH-FAs range from 1.02 μg g^{-1} to 36.0 μg g^{-1}, with the highest concentration in the Bohai Sea, and the lowest in the South China Sea. Generally, the 3-OH-FAs homologues ranged in carbon number from C_{10} to C_{18} with the even numbered C_{12}, C_{14} and C_{16} *normal* homologues and the odd numbered C_{15} *anteiso* homologue typically abundant. *n*-C_{14} was the dominant homologue, except for two samples in the Bering Sea, where the C_{12} compound was slightly more abundant. Notably the odd numbered C_{13}, C_{15} and C_{17} *anteiso* and *iso* isomers were more abundant than their *normal* counterparts. Moreover, the C_{13}, C_{15} and C_{17} homologues showed higher concentrations in the investigated marine sediments, compared to previously studied soil samples (Wang et al., 2016, 2018; Huguet et al., 2019). In addition, the unsaturated C_{18} 3-OH-FA was commonly detected in the marine samples. The 3-OH-FA concentrations in core B3 varied from

5.75 to 9.65 μg g^{-1} (e.g., within the range of concentrations measured in the surface sediments of the ECS).

3-OH-FA based pH and temperature indices were calculated following equations 1–6. The pH indices showed significant variation down-core: Branching Ratio (0.34 to 1.28); Branched Index (0.25 to 0.56); RIAN (–0.11 to 0.47) and RIN (0.23 to 0.84). The temperature proxies RAN_{15} and RAN_{17} varied from 3.27 to 16.3 and 1.82 to 7.50, respectively (Table 1). In core B3, values for these indices fluctuated over the past 57 years (Supplementary Data).

3.3. GDGT distributions in surface and core sediments

The isoGDGTs from both surface sediments and core B3 were measured and the TEX_{86} values were calculated. The concentrations of isoGDGTs from the surface sediments varied from 0.01 to 2.33 μg g^{-1}. The isoGDGT based TEX_{86} values ranged from 0.30 to 0.69, representing a temperature range from 6.0 °C to 27.8 °C when using the global calibration (Kim et al., 2008). The concentration of isoGDGTs ranged from 12.8 to 20.8 ng g^{-1}, with GDGT-0 and crenarchaeol being most abundant in the B3 core. TEX_{86} values ranged from 0.54 to 0.59, yielding reconstructed TEX_{86} temperatures of 20.2–21.7 °C. TEX_{86}^{H} and TEX_{86}^{L} ranged from 0.23 to 0.27 and from 0.35 to 0.40, respectively (Supplementary Data). The TEX_{86}-based temperature calculated in B3 showed a similar trend with the estimates from core PN-2 (Lü et al., 2014) during the last 57 years.

3.4. Statistical analysis

To examine which environmental factors influence 3-OH-FA distributions in marine and soil samples, principal component analysis (PCA) on the fractional abundances of 3-OH-FA homologues was performed. The first two components explain 69% of the variance, with the marine sediments and soils obviously clustered in different biplots (Fig. 4A). On the first principal component (PC1, explaining 44% of the variance) the loading of the marine and soil 3-OH-FAs fall in opposed quadrants, with marine sediments in the right-hand quadrants.

In addition, we performed redundancy analysis (RDA) on the marine surface sedimentary 3-OH-FAs. We used environmental factors, including surface water SST, water depth, salinity, pH, nitrate, phosphate and silicate concentration as an exploratory constraint on their influence on the distribution of 3-OH-FAs in the marine samples. The results show that annual mean SST explains most of the variability in 3-OH-FAs distributions, while other parameters, including pH, seemed to exert insignificant influence on the distributions (Table 2). Although the pH in the marine environment had statistically insignificant influence ($p = 0.17$) on the 3-OH-FA distributions (Table 2), we include it with SST when exploring the influence of environmental factors on 3-OH-FA based proxies (Fig. 4B), due to the known influence of pH on 3-OH-FAs in soil samples (and because it is the second ranked factor after temperature). We found that the pH proxies RIAN, Branching Ratio and RIN are loaded on the first axis of the RDA (RDA1, explaining 32% of the variance), whereas the temperature proxies RAN_{15} and RAN_{17} were loaded on the second axis of RDA (RDA2 (explaining 13% of the variance, Fig. 4B). The RDA results show that the Branched Index, Branching Ratio, RIN are negatively correlated with SST, while RIAN and TEX_{86} show a positive relationship with SST.

4. Discussion

4.1. Distributions of 3-OH-FAs in soils and marine sediments

The distributions of 3-OH-FAs in soils from an altitudinal transect in China (Mt. Shennongjia) were previously investigated and novel pH and temperature proxies were proposed based on indices of *normal*, *iso* and *anteiso* 3-OH-FAs (Wang et al., 2016). Recently, those 3-OH-FA based proxies were shown to be workable in further soil transects from tropical and temperate climate regions (Huguet et al., 2019). However, the correlative relationship between the 3-OH-FA based indices RAN_{15} and RAN_{17} and MAAT previously found in soil transects (Wang et al., 2016; Huguet et al., 2019) was not replicated in our latitudinal transect of marine surface sediments, which covered a large mean annual SST range (1.3–28.1 °C, Supplementary Fig. S1). The RAN_{15} and RAN_{17} values in the marine sediments show higher values than those in soils and do not correlate with SST (Supplementary Fig. S1). These findings imply that these soil-based proxies may be not applicable to marine environments for SST reconstruction, even in marginal settings. Geochemically, this is due to the typical 3-OH-FA isomer fingerprint we measured in marine sediments not having an analogue within the existing soil-based calibrations (Wang et al., 2016; Huguet et al., 2019). Specifically, this is due to the relatively higher abundances of the *a*-C_{15} and *a*-C_{17} isomers in the marine sediments vs soils (Fig. 5A, B).

Furthermore, we explored the relative abundance of the summed *anteiso* vs *normal* and *iso* 3-OH-FAs in marine sediments and soils (Fig. 5C, D), the results reveal that the marine environment produces distinctly higher abundances (> 20% of total 3-OH-FAs) of the *anteiso* 3-OH-FA isomers for most homologues. This is supported by

our PCA analysis, which shows the soil and the marine sediments clustering on different sides in the PCA biplot (Fig. 4A). Consequently, we use a ternary plot to further visualize the distributional differences of the marine vs published soil 3-OH-FAs (Wang et al., 2016; Huguet et al., 2019). The results clearly highlight the different distribution domains: soils contain relatively higher abundances of the higher molecular weight homologues $C_{15\text{-}18}$ 3-OH-FAs (ca. 25–60%), compared to marine samples (ca. 10–35%) (Fig. 6). Marine samples contain higher abundances of all *anteiso* homologues (ca. 10–35%) compared to soil samples (ca. > 10%).

We further investigated correlations between the previously reported 3-OH-FA based terrestrial pH proxies (Branching Ratio, Branched Index, RIAN and RIN) and sea surface water pH (Fig. 7). The relationships were more apparent than for the temperature proxies RAN_{15} and RAN_{17} but were relatively weak, which suggests that the application of terrestrially derived 3-OH-FA based pH proxies is not suitable in the marine environment. We note this relationship needs further investigation. The pH data coverage in the WOA is much more sparse than for temperature, thus pH values in the WOA likely contain greater errors and offsets compared to temperature data. Additionally, the lack of a linear relationship may in part be due to the pH of ocean surface waters being relatively stable and showing only a small range of variation, thus 3-OH-FAs producers may not be so sensitive in a limited pH range (7.4–8.2). Finally, it is fundamentally hard to disentangle temperature from pH as environmental drivers in the global ocean as the two parameters are broadly correlated (Supplementary Fig. S1), due to colder water absorbing more CO_2, driving the carbonate ion balance towards more acidic values.

Interestingly, the four soil pH proxies showed stronger linear relationships with SST rather than pH in our marine samples (Fig. 8), suggesting that 3-OH-FAs distributions in marine environments are more broadly controlled by temperature, whereas 3-OH-FAs distributions in soil are influenced by both temperature and pH changes (where pH ranges are much greater). Indeed, our RDA results confirm that pH did not significantly influence 3-OH-FAs distributions in the marine sediments (Table 2). Hence, distributions of 3-OH-FAs in marine vs soil environments are significantly and distinctly different, and have differing responses to environmental factors. Thus soil-derived 3-OH-FA based proxies are not applicable in marine environments.

4.2. Sources of 3-OH-FAs in soils and marine sediments

A number of terrestrial input proxies including TOC/TON (total organic carbon/ total organic nitrogen), hopanes and higher plant wax biomarkers, BIT (branched isoprenoid tetraether index), TMBR (terrestrial and marine biomarker ratio) and bulk and compound specific $\delta^{13}C$ have been used to constrain organic sources in marginal seas (Hopmans et al., 2004; Pancost and Boot, 2004; Xing et al., 2014) and where terrestrial inputs dominate can be used to reconstruct paleo-terrestrial environments. Specifically, in the West Pacific region studies on the spatial pattern of terrestrial proxies in the Yellow Sea, East China Sea and the Sea of Okhotsk indicate high terrestrial organic matter inputs to this marginal region (Seki et al., 2014; Xing et al., 2014, 2016; Yao et al., 2015).

Most of our samples are derived from marginal basins, with water depths less than 200 m (Table 1) and so it is possible that our marine surface sediment samples could contain relatively high proportions of terrestrially sourced 3-OH-FAs. However, the

fingerprint of 3-OH-FA homologues in our soil and marine sediments show clear differences in distributions (Figs. 4–6). Gram-negative bacteria, the biological precursors of 3-OH-FAs, are the most abundant bacteria in the marine environment (Giovannoni, 2000). Whatever the relative input of marine vs terrestrial 3-OH-FAs, the observed difference in 3-OH-FA distributions (Fig. 6) suggests that the primary marine 3-OH-FA geochemical signature is not overprinted by terrestrial/soil 3-OH-FA derived inputs.

3-OH-FA profiles in the marine water column have been previously investigated in a number of oceanic settings, including the Black Sea, Gulf of Mexico, Equatorial Pacific and North Sea (Kawamura et al., 1987; Wakeham, 1999, 2003). Wakeham (1999) found that 3-OH-FAs were the most abundant hydroxy acid fraction, comprising ca. 100% of total hydroxy fatty acids in marine particulate matter in the Black Sea. 3-OH-FA concentrations were relatively high in the upper water column (top 30 m) and decreased with increasing depth (Wakeham, 1999). Wakeham (1999) concluded that 3-OH-FAs in the Black Sea reflected a direct biosynthetic origin by aqueous microalgae and cyanobacterial LPS (as previously proposed by Matsumoto et al., 1988), including possible contributions from anaerobic and methylotrophic bacteria (given the anoxic conditions of deeper waters and sediments in the Black Sea). More generally, Gram-negative bacteria, the biological precursors of 3-OH-FAs, are the most abundant bacteria in the marine environment (Giovannoni, 2000). Brown et al. (2009) report that both bacterial abundance and species richness are highest in the upper (10 m) of the water column of the oligotrophic North Pacific compared to deeper waters (800 m and 4400 m). Ghiglione et al. (2007) and Liu et al. (2018) found complex relationships between free-living and particle-attached bacterial community abundances at different

depths, but it is noteworthy that Liu et al. (2018) found significantly higher abundances in the upper water column (75 m) of (free-living) Gram-negative alphaproteo-, cyano- and particle-attached deltaproteo-bacteria. Thus, a dominant input of 3-OH-FAs in the marine environment from precursor Gram-negative bacteria dwelling in the upper water column is reasonable. We note that 3-OH-FA acids are also found in seagrasses (Volkman et al., 1980; Gillan et al., 1984; Nichols and Johns, 1985; de Leeuw et al., 1995), but we do not consider this as a viable dominant source beyond the littoral zone.

Our 16S rRNA results give additional direct evidence for different bacterial precursor populations for the 3-OH-FAs measured in marine surface sediments vs soils. In the SCS samples, Proteobacteria account for ca. 94% of all the Gram-negative bacteria at the phylum level, followed by Bacteroidetes (Fig. 9). In sediments from coastal (39 m) to deep basin (3960 m) sites in the SCS, the proportion of Proteobacteria increases from 89% to 97%, which suggests a high contribution of Proteobacteria in open marine settings. In soil samples, the Gram-negative bacteria are dominated by Proteobacteria (ca. 51%) and Acidobacteria (ca. 24%). However, even though Proteobacteria are the dominant Gram-negative bacteria in both our marine sediments and soils (Fig. 9), the composition of Proteobacteria is different at the class level (Supplementary Fig. S2). In marine sediments, Proteobacteria are dominated by alphaproteobacteria and gammaproteobacteria, while in soils the Proteobacteria are dominated by alphaproteobacteria, betaproteobacteria, gammaproteobacteria and deltaproteobacteria (Supplementary Fig. S2). Cho and Giovannoni (2004) successfully purified twelve Gammaproteobacteria, which are physiologically diverse heterotrophs, from coastal and pelagic regions of the Pacific Ocean. The physiological characteristics

of Gammaproteobacteria in the marine environment and whether they are the primary source of marine produced 3-OH-FAs requires further investigation.

In the soil environment, constraining the source of 3-OH-FAs is challenging due to the relatively diverse and complex Gram-negative bacterial community. The most abundant group, Proteobacteria (ca. 51%) may be the main source of 3-OH-FAs in terrestrial environments. Indeed, *Pseudomonas,* a genus of Proteobacteria, yields 3-OH-FAs in terrestrial systems, especially in cave soils, drip waters and stalagmites (Liu et al., 2010; Sardar et al., 2015; Wang et al., 2018). However, due to the observed differences in the distribution of 3-OH-FAs in soils and marine environments (Figs. 4-6), we assume that soil 3-OH-FAs producers include inputs from different Proteobacteria classes (Supplementary Fig. S2). In addition, contributions from Acidobacteria (ca. 24%) in soils as a source of a proportion of the 3-OH-FAs cannot be excluded. Acidobacteria are the most abundant Gram-negative bacterial community except for Proteobacteria in soils (Fig. 9), which is mainly influenced by pH, temperature and elevation (Shen et al., 2019). Acidobacteria have been suggested as a potential source for bacterial GDGTs (brGDGTs) in soil environments (Sinninghe Damsté et al., 2014). Interestingly, Wang et al. (2016) showed that the 3-OH-FA-based temperature and pH indices have a good linear relationship with brGDGT-derived proxies from the same altitudinal soil transect in central China. Whether this robust linear relationship between the 3-OH-FA and brGDGT-based proxies represents similar biological sources requires further analysis.

Overall, we present multiple lines of evidence which demonstrate different distributions and sources of 3-OH-FAs in soils vs marine surface sediments. Our PCA analysis (Fig. 4A) and ternary plot (Fig. 6) highlight that marine and soil 3-OH-FA

distributions are distinct, and specifically that marine sediments contain relatively higher abundances of *anteiso* 3-OH-FAs and soils contain relatively higher abundances of lower molecular weight 3-OH-FAs (C_{10}-C_{14}; Fig. 6). The correlation between our 3-OH-FA distributions (see RAN_{13} below) with satellite SSTs and the observation of the highest water column abundance of many Gram-negative bacterial groups and 3-OH-FAs in the upper water column (Wakeham, 1999) supports a predominantly upper water column origin (e.g., surface to deep chlorophyll maximum) for the marine sedimentary 3-OH-FA signal. We propose that this signal is mainly transported to sediments by means of fecal pellet packaging, mineral ballast and aggregation into larger particles (e.g., marine snow), since bacterial cells are too small and low in density to sink independently.

Finally, the genetic evidence suggests that the 3-OH-FA producers in our marine samples are mainly derived from alphaproteobacteria and gammaproteobacteria, while in soils, alphaproteobacteria, betaproteobacteria, gammaproteobacteria, deltaproteobacteria and acidobacteria present a more diverse population of possible 3-OH-FAs producers (Supplementary Fig. S2). Much future work is required, including characterization of particulate organic matter in the water column, mesocosms, culture experiments and genetic analysis to constrain and decipher 3-OH-FA sources in terrestrial and marine environments and in different geological archives.

4.3. RAN_{13} – a novel SST index based on 3-OH-FAs

In marine environments, bacterial communities may be affected by temperature, salinity, water pH, redox conditions and nutrient conditions (nitrate, phosphate and silicate concentrations). Our RDA analysis of marine 3-OH-FAs distributions and

environmental factors indicates that annual mean SST is the key factor controlling the 3-OH-FAs distributions (Table 2). We find marine samples contain higher abundances of *iso* and *anteiso* C_{13} 3-OH-FAs compared with soils. Intriguingly, the abundance of *iso* and *anteiso* C_{13} 3-OH-FAs appears to vary systematically across the latitudinal range of the sampled ocean basins (Fig. 3 and Supplementary Data). For example, the *iso* and *anteiso* C_{13} 3-OH-FAs show lower abundances (ca. 5%) in the South China Sea than in the mid-latitude Yellow Sea (ca. 10%) and the high-latitude Bering Sea (ca. 15%; Supplementary Data).

Here we propose a new proxy using the ratio of *anteiso* to *normal* C_{13} 3-OH-FA (RAN_{13}), RAN_{13} defined as follows:

$$RAN_{13} = a\text{-}C_{13}/n\text{-}C_{13}\ 3\text{-OH-FA} \quad (13)$$

From the RDA results, we find that RAN_{13} is strongly influenced by SST (Fig. 4B). Indeed, there is a strong exponential relationship between RAN_{13} and SST in our dataset across a temperature range of 1.3 °C to 28.1 °C (Fig. 10A). RAN_{13} values decrease with increasing SST, with the lowest value in the South China Sea (0.73, 27.5 °C, 12.1 °N) and highest value in the Bering Sea (7.09, 2.1 °C, 62.8 °N). This negative relationship between RAN_{13} and SST is comparable to that of RAN_{15} (RAN_{17}) and MAAT in soils. This common response of 3-OH-FAs to temperature likely reflects the same fundamental mechanistic response of certain Gram-negative bacterial groups to temperature change. Specifically, bacteria likely increase the proportion of *anteiso* 3-OH-FAs with decreasing temperature in order to maintain membrane fluidity, as the *anteiso* fatty acids have a notably lower melting point (ca. 30 °C) than both *normal* and *iso* fatty acids (Kaneda, 1991; Suutari and Laakso, 1994). Interestingly, the RAN_{13} proxy in soil samples shows no correlation with the MAATs from the published data

(Supplementary Fig. S1) (Wang et al., 2016, 2018; Huguet et al., 2019). This suggests that different Gram-negative bacterial groups in marine sediments vs soils may use different compounds in response to environmental changes. The RAN_{13} index seems to be an independent marine temperature proxy, which is not greatly affected or overprinted by terrestrial signals, even in marginal basins.

The GDGT-based TEX_{86} has been widely used as a temperature proxy in the global oceans, showing a linear relationship over a wide range of temperatures (Schouten et al., 2013). The RAN_{13} index in our dataset also shows an exponential relationship with TEX_{86}-derived SSTs in the same samples ($R^2 = 0.37$, $p < 0.001$, n = 31; Fig. 10B). The relatively lower correlation between the two proxies may be due to the overestimate of temperatures by TEX_{86} in lower-SST region, for example the Bering Sea, where the SSTs are under 5 °C (Fig. 10B). Kim et al. (2010) suggested that the relative abundance of the regio-isomer of crenarchaeol may not have a strong correlation with lower SSTs. For more accurate estimates of SST, the TEX_{86}^{H} (the logarithmic function of TEX_{86}) and TEX_{86}^{L} (the logarithmic function excluding the crenarchaeol regio-isomer) were promoted for calibration the SST in high and low temperature regions, respectively (Kim et al., 2010). We explored these two temperature proxies, as well as the RAN_{13} with satellite SSTs in tropical (> 25 °C) and polar surface sediments (< 6 °C), to test the application of RAN_{13} proxy. The results showed that the calibration of TEX_{86}^{H} in higher temperatures ($R^2 = 0.53$, n = 7, $p < 0.001$) is slightly weaker than that of RAN_{13} with SSTs ($R^2 = 0.69$, n = 7, $p < 0.001$; Fig. 10C). Similarly, the TEX_{86}^{L} showed a poor relationship with SSTs ($R^2 = 0.16$, n = 10; Fig. 10D) under 6 °C (most being Bering Sea surface sediments). The complicated seasonal ocean currents in the Bering Sea may partly explain the insensitivity of the GDGT-based

TEX_{86}^{L} to temperature changes (Grebmeier et al., 2006). In contrast, the RAN_{13} presents a strong relationship with SSTs ($R^2 = 0.55$, Fig. 10D), even at lower temperatures, which highlights the potential of using RAN_{13} as a temperature proxy in tropical to polar oceans.

Thus, we propose an exponential relationship of RAN_{13} with SSTs and obtained the following equations for temperature calibration.

$SST = \exp \wedge (3.75 - 0.47 \times RAN_{13})$ ($R^2 = 0.92$, $p < 0.001$, RMSE = 2.55) (14)

We also calculated the residual SSTs (the temperature difference between RAN_{13} and observed satellite SSTs) (Fig. 11B). These residuals fall well within the residual error lines except for several samples in tropical oceans, which may partly be biased by the relative lower abundance of 3-OH-FAs in that regions. The good overall performance of the RAN_{13} calibration, especially at the low end of the SST spectrum, suggests the exponential calibration of RAN_{13} could be a robust proxy for tropical and polar ocean palaeo-temperature reconstruction.

4.4. Comparison of a RAN_{13} based SST reconstruction with instrumental-era data.

Box core B3 contains a high-resolution marine record of climate since about 1959. We use this sedimentary record, which overlaps with the instrumental and satellite era of climate observation, to test the application of the RAN_{13} temperature proxy during the past 57 years. We calculated the mean annual SST at site B3 since the 1950s (mean temperature ca. 20.0 °C) (Fig. 12C). RAN_{13} temperatures were reconstructed using the exponential Eq. 14. Temperatures fluctuated from 16.6 °C to 23.3 °C (average 20.2 °C), during the past 57 years. The RAN_{13} calculated SST trends were remarkably close to instrumental SSTs, recording a longer-term temperature

increase from 1960 to 2017. Superimposed on this are sub-decadal fluctuations of ca. 4 °C, especially notable are oscillations during the 1970s to 1980s, and the persistent SST increase from the 1990s (which are observed in the instrumental SSTs). In addition, we compared our data with TEX_{86} data from the same core (B3 – this study) and with published TEX_{86} data from proximal core PN-2 in the ECS (Lü et al., 2014). The TEX_{86}^{H}-based temperatures ranged from 20.2 °C to 21.7 °C (average 21.0 °C; Fig. 12E). The average down-core TEX_{86} temperatures are statistically indistinguishable from the RAN_{13}-SSTs (although slightly higher than the average instrumental and RAN_{13}-derived temperatures). However, in comparison to the RAN_{13} proxy, TEX_{86} does not reconstruct either the longer-term warming trend observed in the instrumental data or the sub-decadal oscillations with the same fidelity (Fig. 12). As noted above the RAN_{13}-SSTs pick out strong sub-decadal changes, observed in the instrumental data and likely related to El Niño and La Niña events, as well as the Pacific decadal oscillation (PDO). In a positive phase the PDO brings warmer SSTs and MAAT (via the strengthening of the Kuroshio current) to the East Asia (Wang et al., 2008; Yao et al., 2018). This appears to be reflected in both our RAN_{13}-SSTs and the terrestrial MBT/CBT-MAATs from the ECS (Fig. 12).

Both the relationship of RAN_{13} to satellite SSTs in surface marine sediments and the agreement between down-core derived SSTs and instrumental SSTs in core B3 suggest that RAN_{13} could be used to reconstruct temperature changes. Our results imply that the highly seasonal inputs of terrestrial organic matter in the Western Pacific marginal seas do not overprint marine 3-OH-FAs distributions and RAN_{13}-based mean annual SSTs. Thus, the present study demonstrates both the first calibration of the 3-

OH-FA RAN_{13} SST proxy and how this biomarker tool can reconstruct past SST signals in marine sediments.

5. Conclusions

We investigated 3-OH-FA distributions in a marginal marine surface sediment transect from the western North Pacific Ocean. We identified significantly different distributions and sources of 3-OH-FAs in marine sediments vs soils via both empirical/statistical and genetic analysis. Marine sediments contain higher relative abundances of *anteiso* 3-OH-FAs. 3-OH-FAs producers in the marine environment are likely alphaproteobacteria and gammaproteobacteria, while microbial producers in the soil are likely a mix of alphaproteobacteria, betaproteobacteria, gammaproteobacteria, deltaproteobacteria and acidobacteria. The soil temperature proxies RAN_{15} and RAN_{17} showed no linear relationship with SST. We propose a new independent marine bacterial temperature proxy, RAN_{13}, which shows a strong exponential relationship with satellite SSTs in our dataset. We suggest that the RAN_{13} signal originates with precursor Gram-negative bacteria dwelling in the upper water column. We demonstrate that RAN_{13}-derived temperatures from sediment core B3 agree with instrumental SSTs over the last 57 years. Thus, the present study demonstrates both the first calibration of the 3-OH-FA RAN_{13} SST proxy and how this biomarker tool can reconstruct past SST signals in marine sediments.

Acknowledgements

We thank the Editors Dr George Wolff and Dr John Volkman and two anonymous reviewers for their constructive comment to improve the quality of this

manuscript. We thank Prof. Weidong Zhai and Dr. Shu Yang for surface sediments from Yellow Sea and Bohai Sea, Dr. Li Lo and Sergey A. Gorbarenko for three Okhotsk Sea surface sediments, and Dr. Limin Hu for surface sediments from Japan Sea and Okhotsk Sea. Thanks to Dr. Xing Xiang for helping with the BugBase analysis. This work was supported by the National Natural Science Foundation of China (grant nos. 41807419, 41821001, 41830319), the Key R&D Project of Ministry of Science and Technology (grant no. 2016YFA0601100), the 111 project (National Bureau of Foreign Experts and the Ministry of Education of China; grant no. B08030), and the Fundamental Research Funds for the National Universities, China University of Geosciences, Wuhan (grant no. CUGL170815).

Competing interest statement

The authors declare no competing interests.

Associate Editor–**George Wolff**

References

Bahram, M., Hildebrand, F., Forslund, S.K., Anderson, J.L., Soudzilovskaia, N.A., Bodegom, P.M., Bengtsson-Palme, J., Anslan, S., Coelho, L.P., Harend, H., Huerta-Cepas, J., Medema, M.H., Maltz, M.R., Mundra, S., Olsson, P.A., Pent, M., Polme, S., Sunagawa, S., Ryberg, M., Tedersoo, L., Bork, P., 2018. Structure and function of the global topsoil microbiome. Nature 560, 233–237.

Bergmann, G.T., Bates, S.T., Eilers, K.G., Lauber, C.L., Caporaso, J.G., Walters, W.A., Knight, R., Fierer, N., 2011. The under-recognized dominance of *Verrucomicrobia* in soil bacterial communities. Soil Biology and Biochemistry 43, 1450–1455.

Bijl, P.K., Bendle, J.A., Bohaty, S.M., Pross, J., Schouten, S., Tauxe, L., Stickley, C.E., McKay, R.M., Röhl, U., Olney, M., 2013. Eocene cooling linked to early flow across the Tasmanian Gateway. Proceedings of the National Academy of Sciences 110, 9645–9650.

Brassell, S., Eglinton, G., Marlowe, I., Pflaumann, U., Sarnthein, M., 1986. Molecular stratigraphy: a new tool for climatic assessment. Nature 320, 129–133.

Brown, M.V., Philip, G.K., Bunge, J.A., Smith, M.C., Bissett, A., Lauro, F.M., Fuhrman, J.A., Donachie, S.P., 2009. Microbial community structure in the North Pacific ocean. The ISME Journal 3, 1374.

Caporaso, J.G., Kuczynski, J., Stombaugh, J., Bittinger, K., Bushman, F.D., Costello, E.K., Fierer, N., Pena, A.G., Goodrich, J.K., Gordon, J.I., 2010. QIIME allows analysis of high-throughput community sequencing data. Nature Methods 7, 335–336.

Caporaso, J.G., Lauber, C.L., Walters, W.A., Berg-Lyons, D., Lozupone, C.A., Turnbaugh, P.J., Fierer, N., Knight, R., 2011. Global patterns of 16S rRNA diversity at a depth of millions of sequences per sample. Proceedings of the National Academy of Sciences 108, 4516–4522.

Chen, B., Fan, D., Li, W., Wang, L., Zhang, X., Liu, M., Guo, Z., 2014. Enrichment of heavy metals in the inner shelf mud of the East China Sea and its indication to human activity. Continental Shelf Research 90, 163–169.

Chen, L., Liu, J., Xing, L., Krauss, K.W., Wang, J., Xu, G., Li, L., 2017. Historical changes in organic matter input to the muddy sediments along the Zhejiang-Fujian Coast, China over the past 160 years. Organic Geochemistry 111, 13–25.

Cho, J.-C., Giovannoni, S.J., 2004. Cultivation and growth characteristics of a diverse group of oligotrophic marine *Gammaproteobacteria*. Applied and Environmental Microbiology 70, 432–440.

Cole, J.R., Wang, Q., Cardenas, E., Fish, J., Chai, B., Farris, R.J., Kulam-Syed-Mohideen, A.S., McGarrell, D.M., Marsh, T., Garrity, G.M., Tiedje, J.M., 2009. The Ribosomal Database Project: improved alignments and new tools for rRNA analysis. Nucleic Acids Research 37, 141–145.

Conte, M.H., Sicre, M.A., Rühlemann, C., Weber, J.C., Schulte, S., Schulz-Bull, D., Blanz, T., 2006. Global temperature calibration of the alkenone unsaturation index ($U_{37}^{K'}$) in surface waters and comparison with surface sediments. Geochemistry, Geophysics, Geosystems 7(2). https://doi.org/10.1029/2005GC001054.

Cranwell, P., 1981. Diagenesis of free and bound lipids in terrestrial detritus deposited in a lacustrine sediment. Organic Geochemistry 3, 79–89.

de Bar, M.W., Dorhout, D.J., Hopmans, E.C., Rampen, S.W., Sinninghe Damsté, J.S., Schouten, S., 2016. Constraints on the application of long chain diol proxies in the Iberian Atlantic margin. Organic Geochemistry 101, 184–195.

de Bar, M.W., Rampen, S.W., Hopmans, E.C., Sinninghe Damsté, J.S., Schouten, S., 2019. Constraining the applicability of organic paleotemperature proxies for the last 90 Myrs. Organic Geochemistry 128, 122–136.

de Leeuw, J.W., Rijpstra, W.I.C., Nienhuis, P.H., 1995. Free and bound fatty acids and hydroxy fatty acids in the living and decomposing eelgrass *Zostera marina* L. Organic Geochemistry 23, 721–728.

Denich, T.J., Beaudette, L.A., Lee, H., Trevors, J.T., 2003. Effect of selected environmental and physico-chemical factors on bacterial cytoplasmic membranes. Journal of Microbiological Methods 52, 149–182.

Eglinton, G., Hamilton, R.J., 1967. Leaf epicuticular waxes. Science 156, 1322.

Eley, Y.L., Thompson, W., Greene, S.E., Mandel, I., Edgar, K., Bendle, J.A., Dunkley Jones, T., 2019. OPTiMAL: A new machine learning approach for GDGT-based palaeothermometry. Climate of the Past Discussions, https://doi.org/10.5194/cp-2019-60.

Elling, F.J., Könneke, M., Mußmann, M., Greve, A., Hinrichs, K.-U., 2015. Influence of temperature, pH, and salinity on membrane lipid composition and TEX_{86} of marine planktonic thaumarchaeal isolates. Geochimica et Cosmochimica Acta 171, 238–255.

Eltgroth, M.L., Watwood, R.L., Wolfe, G.V., 2005. Production and cellular localization of neutral long-chain lipids in the haptophyte algae *Isochrysis galbana* and *Emiliania huxleyi*. Journal of Phycology 41, 1000–1009.

Epstein, B.L., D'Hondt, S., Quinn, J.G., Zhang, J., Hargraves, P.E., 1998. An effect of dissolved nutrient concentrations on alkenone-based temperature estimates. Paleoceanography 13, 122–126.

Fujine, K., Yamamoto, M., Tada, R., Kido, Y., 2006. A salinity-related occurrence of a novel alkenone and alkenoate in Late Pleistocene sediments from the Japan Sea. Organic Geochemistry 37, 1074–1084.

Ghiglione, J., Mevel, G., Pujo-Pay, M., Mousseau, L., Lebaron, P., Goutx, M., 2007. Diel and seasonal variations in abundance, activity, and community structure of particle-attached and free-living bacteria in NW Mediterranean Sea. Microbial Ecology 54, 217–231.

Gillan, F.T., Hogg, R.W., Drew, E.A., 1984. The sterol and fatty acid compositions of seven tropical seagrasses from North Queensland, Australia. Phytochemistry 23, 2817–2821.

Giovannoni, S., 2000. Evolution, diversity and molecular ecology of marine prokaryotes. In: Kirchman, D.L. (Ed.), Microbial Ecology of the Oceans. Wiley, pp. 47–84.

Goossens, H., Irene, W., Rijpstra, C., Düren, R., de Leeuw, J., Schenck, P., 1986. Bacterial contribution to sedimentary organic matter; a comparative study of lipid moieties in bacteria and recent sediments. Organic Geochemistry 10, 683–696.

Grebmeier, J.M., Cooper, L.W., Feder, H.M., Sirenko, B.I., 2006. Ecosystem dynamics of the Pacific-influenced northern Bering and Chukchi Seas in the Amerasian Arctic. Progress in Oceanography 71, 331–361.

Hedrick, D.B., Peacock, A.D., Lovley, D.R., Woodard, T.L., Nevin, K.P., Long, P.E., White, D.C., 2009. Polar lipid fatty acids, LPS-hydroxy fatty acids, and respiratory quinones of three *Geobacter* strains, and variation with electron acceptor. Journal of Industrial Microbiology and Biotechnology 36, 205–209.

Herbert, T.D., 2003. Alkenone paleotemperature determinations. Treatise on Geochemistry 6, 391–432.

Herbert, T.D., Lawrence, K.T., Tzanova, A., Peterson, L.C., Caballero-Gill, R., Kelly, C.S., 2016. Late Miocene global cooling and the rise of modern ecosystems. Nature Geoscience 9, 843–847.

Herbert, T.D., Peterson, Liu, Z., 2010. Tropical ocean temperatures over the past 3.5 million years. Science 328, 1530–1534.

Herbert, T.D., Schuffert, J.D., 1998. Alkenone unsaturation estimates of late Miocene through late Pliocene sea-surface temperatures at Site 958. Proceedings of the Ocean Drilling Program – Scientific Results 159, 17–21.

Herfort, L., Schouten, S., Boon, J.P., Sinninghe Damsté, J.S., 2006. Application of the TEX_{86} temperature proxy to the southern North Sea. Organic Geochemistry 37, 1715–1726.

Hernández-Sánchez, M., Woodward, E., Taylor, K., Henderson, G., Pancost, R., 2014. Variations in GDGT distributions through the water column in the South East Atlantic Ocean. Geochimica et Cosmochimica Acta 132, 337–348.

Hopmans, E.C., Weijers, J.W., Schefuß, E., Herfort, L., Sinninghe Damsté, J.S., Schouten, S., 2004. A novel proxy for terrestrial organic matter in sediments based on branched and isoprenoid tetraether lipids. Earth and Planetary Science Letters 224, 107–116.

Huguet, A., Coffinet, S., Roussel, A., Gayraud, F., Anquetil, C., Bergonzini, L., Bonanomi, G., Williamson, D., Majule, A., Derenne, S., 2019. Evaluation of 3-hydroxy fatty acids as a pH and temperature proxy in soils from temperate and tropical altitudinal gradients. Organic Geochemistry 129, 1–13.

Inglis, G.N., Farnsworth, A., Lunt, D., Foster, G.L., Hollis, C.J., Pagani, M., Jardine, P.E., Pearson, P.N., Markwick, P., Galsworthy, A.M., 2015. Descent toward the

Icehouse: Eocene sea surface cooling inferred from GDGT distributions. Paleoceanography and Paleoclimatology 30, 1000–1020.

Jenske, R., Vetter, W., 2008. Gas chromatography/electron-capture negative ion mass spectrometry for the quantitative determination of 2- and 3-hydroxy fatty acids in bovine milk fat. Journal of Agricultural and Food Chemistry 56, 5500–5505.

Kaneda, T., 1991. Iso- and anteiso-fatty acids in bacteria: biosynthesis, function, and taxonomic significance. Microbiological Reviews 55, 288–302.

Kawamura, K., Ishiwatari, R., Ogura, K., 1987. Early diagenesis of organic matter in the water column and sediments: microbial degradation and resynthesis of lipids in Lake Haruna. Organic Geochemistry 11, 251–264.

Kim, J.-H., Schouten, S., Hopmans, E.C., Donner, B., Sinninghe Damsté, J.S., 2008. Global sediment core-top calibration of the TEX_{86} paleothermometer in the ocean. Geochimica et Cosmochimica Acta 72, 1154–1173.

Kim, J.-H., Van der Meer, J., Schouten, S., Helmke, P., Willmott, V., Sangiorgi, F., Koç, N., Hopmans, E.C., Sinninghe Damsté, J.S., 2010. New indices and calibrations derived from the distribution of crenarchaeal isoprenoid tetraether lipids: Implications for past sea surface temperature reconstructions. Geochimica et Cosmochimica Acta 74, 4639–4654.

Kim, J.H., Schouten, S., Rodrigo-Gámiz, M., Rampen, S., Marino, G., Huguet, C., Helmke, P., Buscail, R., Hopmans, E.C., Pross, J., 2015. Influence of deep-water derived isoprenoid tetraether lipids on the TEX_{86}^{H} paleothermometer in the Mediterranean Sea. Geochimica et Cosmochimica Acta 150, 125–141.

Kim, J.H., Villanueva, L., Zell, C., Sinninghe Damsté, J.S., 2016. Biological source and provenance of deep-water derived isoprenoid tetraether lipids along the Portuguese continental margin. Geochimica et Cosmochimica Acta 172, 177–204.

Lin, T., Nizzetto, L., Guo, Z., Li, Y., Li, J., Zhang, G., 2016. DDTs and HCHs in sediment cores from the coastal East China Sea. Science of the Total Environment 539, 388–394.

Lipp, J.S., Hinrichs, K.-U., 2009. Structural diversity and fate of intact polar lipids in marine sediments. Geochimica et Cosmochimica Acta 73, 6816–6833.

Liu, Q., Wang, H., Zhao, R., Qiu, X., Gong, L., 2010. Bacteria isolated from dripping water in the oligotrophic Heshang cave in central China. Journal of Earth Science 21, 325–328.

Liu, R., Wang, L., Liu, Q., Wang, Z., Li, Z., Fang, J., Zhang, L., Luo, M., 2018. Depth-resolved distribution of particle-attached and free-living bacterial communities in the water column of the New Britain Trench. Frontiers in Microbiology 9, https://doi.org/10.3389/fmicb.2018.00625.

Lopes dos Santos, R.A., Spooner, M.I., Barrows, T.T., De Deckker, P., Sinninghe Damsté, J.S., Schouten, S., 2013. Comparison of organic ($U^{K'}_{37}$, TEX^{H}_{86}, LDI) and faunal proxies (foraminiferal assemblages) for reconstruction of late Quaternary sea surface temperature variability from offshore southeastern Australia. Paleoceanography 28, 377–387.

Lü, X., Yang, H., Song, J., Versteegh, G.J.M., Li, X., Yuan, H., Li, N., Yang, C., Yang, Y., Ding, W., 2014. Sources and distribution of isoprenoid glycerol dialkyl glycerol tetraethers (GDGTs) in sediments from the east coastal sea of China:

Application of GDGT-based paleothermometry to a shallow marginal sea. Organic Geochemistry 75, 24–35.

Magoc, T., Salzberg, S.L., 2011. FLASH: fast length adjustment of short reads to improve genome assemblies. Bioinformatics 27, 2957–2963.

Matsumoto, G.I., Watanuki, K., Torii, T., 1988. Hydroxy acids in Antarctic lake sediments and their geochemical significance. Organic Geochemistry 13, 785–790.

Moossen, H., Bendle, J., Seki, O., Quillmann, U., Kawamura, K., 2015. North Atlantic Holocene climate evolution recorded by high-resolution terrestrial and marine biomarker records. Quaternary Science Reviews 129, 111–127.

Naafs, B.D.A., Hefter, J., Stein, R., 2012. Application of the long chain diol index (LDI) paleothermometer to the early Pleistocene (MIS 96). Organic Geochemistry 49, 83–85.

Nichols, P.D., Johns, R., 1985. Lipids of the tropical seagrass *Thallassia hemprichii*. Phytochemistry 24, 81–84.

Niu, C., Kebede, H., Auld, D.L., Woodward, J.E., Burow, G., Wright, R.J., 2008. A safe inexpensive method to isolate high quality plant and fungal DNA in an open laboratory environment. African Journal of Biotechnology 7, 2818–2822.

Oldfield, F., Appleby, P.G., Battarbee, R.W., 1978. Alternative ^{210}Pb dating: results from the New Guinea Highlands and Lough Erne. Nature 271, 339–342.

Oyaizu, H., Komagata, K., 1983. Grouping of *Pseudomonas* species on the basis of cellular fatty acid composition and the quinone system with special reference to the existence of 3-hydroxy fatty acids. The Journal of General and Applied Microbiology 29, 17–40.

Pancost, R.D., Boot, C.S., 2004. The palaeoclimatic utility of terrestrial biomarkers in marine sediments. Marine Chemistry 92, 239–261.

Raetz, C.R., Reynolds, C.M., Trent, M.S., Bishop, R.E., 2007. Lipid A modification systems in gram-negative bacteria. Annual Review of Biochemistry 76, 295–329.

Rampen, S.W., Willmott, V., Kim, J.H., Uliana, E., Mollenhauer, G., Schefuß, E., Sinninghe Damsté, J.S., Schouten, S., 2012. Long chain 1,13- and 1,15-diols as a potential proxy for palaeotemperature reconstruction. Geochimica et Cosmochimica Acta 84, 204–216.

Robinson, S.A., Ruhl, M., Astley, D.L., Naafs, B.D.A., Farnsworth, A.J., Bown, P.R., Jenkyns, H.C., Lunt, D.J., O'Brien, C., Pancost, R.D., 2017. Early Jurassic North Atlantic sea-surface temperatures from TEX_{86} palaeothermometry. Sedimentology 64, 215–230.

Rodrigo-Gámiz, M., Martínez-Ruiz, F., Rampen, S.W., Schouten, S., Sinninghe Damsté, J.S., 2014. Sea surface temperature variations in the western Mediterranean Sea over the last 20 kyr: A dual-organic proxy ($U_{37}^{K'}$ and LDI) approach. Paleoceanography 29, 87–98.

Rosell-Melé, A., Prahl, F.G., 2013. Seasonality of $U_{37}^{K'}$ temperature estimates as inferred from sediment trap data. Quaternary Science Reviews 72, 128–136.

Sardar, R.K., Kavita, K., Jha, B., 2015. Lipopolysaccharide of *Marinobacter litoralis* inhibits swarming motility and biofilm formation in *Pseudomonas aeruginosa* PA01. Carbohydrate Polymers 123, 468–475.

Schouten, S., Hopmans, E.C., Sinninghe Damsté, J.S., 2004. The effect of maturity and depositional redox conditions on archaeal tetraether lipid palaeothermometry. Organic Geochemistry 35, 567–571.

Schouten, S., Hopmans, E.C., Schefuß, E., Sinninghe Damsté, J.S., 2002. Distributional variations in marine crenarchaeotal membrane lipids: a new tool for reconstructing ancient sea water temperatures? Earth and Planetary Science Letters 204, 265–274.

Seki, O., Bendle, J.A., Harada, N., Kobayashi, M., Sawada, K., Moossen, H., Inglis, G.N., Nagao, S., Sakamoto, T., 2014. Assessment and calibration of TEX_{86} paleothermometry in the Sea of Okhotsk and sub-polar North Pacific region: Implications for paleoceanography. Progress in Oceanography 126, 254–266.

Shen, C., Shi, Y., Fan, K., He, J.-S., Adams, J.M., Ge, Y., Chu, H., 2019. Soil pH dominates elevational diversity pattern for bacteria in high elevation alkaline soils on the Tibetan Plateau. FEMS Microbiology Ecology 95, fiz003.

Sikes, E.L., O'Leary, T., Nodder, S.D., Volkman, J.K., 2005. Alkenone temperature records and biomarker flux at the subtropical front on the Chatham Rise, SW Pacific Ocean. Deep Sea Research Part I: Oceanographic Research Papers 52, 721–748.

Sikes, E.L., Volkman, J.K., Robertson, L.G., Pichon, J.-J., 1997. Alkenones and alkenes in surface waters and sediments of the Southern Ocean: Implications for paleotemperature estimation in polar regions. Geochimica et Cosmochimica Acta 61, 1495–1505.

Sinninghe Damsté, J.S., Rijpstra, W.I.C., Hopmans, E.C., Foesel, B.U., Wüst, P.K., Overmann, J., Tank, M., Bryant, D.A., Dunfield, P.F., Houghton, K., Stott, M.B., 2014. Ether- and ester-bound *iso*- diabolic acid and other lipids in members of *Acidobacteria* subdivision 4. Applied and Environmental Microbiology 80, 5207–5218.

Suutari, M., Laakso, S., 1994. Microbial fatty acids and thermal adaptation. Critical Reviews in Microbiology 20, 285–328.

Taylor, K.W., Huber, M., Hollis, C.J., Hernandez-Sanchez, M.T., Pancost, R.D., 2013. Re-evaluating modern and Palaeogene GDGT distributions: Implications for SST reconstructions. Global and Planetary Change 108, 158–174.

Tierney, J.E., Tingley, M.P., 2018. BAYSPLINE: A new calibration for the alkenone paleothermometer. Paleoceanography and Paleoclimatology 33, 281–301.

Trommer, G., Siccha, M., van der Meer, M.T., Schouten, S., Sinninghe Damsté, J.S., Schulz, H., Hemleben, C., Kucera, M., 2009. Distribution of Crenarchaeota tetraether membrane lipids in surface sediments from the Red Sea. Organic Geochemistry 40, 724–731.

Tyagi, P., Ishimura, Y., Kawamura, K., 2015. Hydroxy fatty acids in marine aerosols as microbial tracers: 4-year study on β- and ω-hydroxy fatty acids from remote Chichijima Island in the western North Pacific. Atmospheric Environment 115, 89–100.

Versteegh, G., de Leeuw, J., Taricco, C., Romero, A., 2007. Temperature and productivity influences on $U^{K'}_{37}$ and their possible relation to solar forcing of the Mediterranean winter. Geochemistry, Geophysics, Geosystems 8.

Villanueva, L., Schouten, S., Sinninghe Damsté, J.S., 2015. Depth-related distribution of a key gene of the tetraether lipid biosynthetic pathway in marine Thaumarchaeota. Environmental Microbiology 17, 3527–3539.

Volkman, J., Johns, R., Gillan, F., Perry, G., Bavor Jr, H., 1980. Microbial lipids of an intertidal sediment—I. Fatty acids and hydrocarbons. Geochimica et Cosmochimica Acta 44, 1133–1143.

Volkman, J.K., Barrett, S.M., Blackburn, S.I., Sikes, E.L., 1995. Alkenones in *Gephyrocapsa oceanica*: implications for studies of paleoclimate. Geochimica et Cosmochimica Acta 59, 513–520.

Wakeham, S.G., 1999. Monocarboxylic, dicarboxylic and hydroxy acids released by sequential treatments of suspended particles and sediments of the Black Sea. Organic Geochemistry 30, 1059–1074.

Wakeham, S.G., Pease, T.K., Benner, R., 2003. Hydroxy fatty acids in marine dissolved organic matter as indicators of bacterial membrane material. Organic Geochemistry 34, 857–868.

Wang, C., Bendle, J., Yang, Y., Yang, H., Sun, H., Huang, J., Xie, S., 2016. Impacts of pH and temperature on soil bacterial 3-hydroxy fatty acids: Development of novel terrestrial proxies. Organic Geochemistry 94, 21–31.

Wang, C., Bendle, J.A., Zhang, H., Yang, Y., Liu, D., Huang, J., Cui, J., Xie, S., 2018. Holocene temperature and hydrological changes reconstructed by bacterial 3-hydroxy fatty acids in a stalagmite from central China. Quaternary Science Reviews 192, 97–105.

Wang, C., Zhang, H., Huang, X., Huang, J., Xie, S., 2012. Optimization of acid digestion conditions on the extraction of fatty acids from stalagmites. Frontiers of Earth Science 6, 109–114.

Wang, L., Chen, W., Huang, R., 2008. Interdecadal modulation of PDO on the impact of ENSO on the East Asian winter monsoon. Geophysical Research Letters 35.

Wang, Q., Garrity, G.M., Tiedje, J.M., Cole, J.R., 2007. Naïve Bayesian classifier for rapid assignment of rRNA sequences into the new bacterial taxonomy. Applied and Environmental Microbiology 73, 5261–5267.

Ward, T., Larson, J., Meulemans, J., Hillmann, B., Lynch, J., Sidiropoulos, D., Spear, J., Caporaso, G., Blekhman, R., Knight, R., 2017. BugBase predicts organism level microbiome phenotypes. BioRxiv, 133462.

Wei, Y., Wang, J., Liu, J., Dong, L., Li, L., Wang, H., Wang, P., Zhao, M., Zhang, C.L., 2011. Spatial variations in archaeal lipids of surface water and core-top sediments in the South China Sea and their implications for paleoclimate studies. Applied and Environmental Microbiology 77, 7479–7489.

Weijers, J.W., Schouten, S., Spaargaren, O.C., Sinninghe Damsté, J.S., 2006. Occurrence and distribution of tetraether membrane lipids in soils: Implications for the use of the TEX_{86} proxy and the BIT index. Organic Geochemistry 37, 1680–1693.

Xing, L., Hou, D., Wang, X., Li, L., Zhao, M., 2016. Assessment of the sources of sedimentary organic matter in the Bohai Sea and the northern Yellow Sea using biomarker proxies. Estuarine, Coastal and Shelf Science 176, 67–75.

Xing, L., Zhao, M., Gao, W., Wang, F., Zhang, H., Li, L., Liu, J., Liu, Y., 2014. Multiple proxy estimates of source and spatial variation in organic matter in surface sediments from the southern Yellow Sea. Organic Geochemistry 76, 72–81.

Xu, B., Bianchi, T.S., Allison, M.A., Dimova, N.T., Wang, H., Zhang, L., Diao, S., Jiang, X., Zhen, Y., Yao, P., 2015. Using multi-radiotracer techniques to better understand sedimentary dynamics of reworked muds in the Changjiang River estuary and inner shelf of East China Sea. Marine Geology 370, 76–86.

Yamamoto, M., Shimamoto, A., Fukuhara, T., Naraoka, H., Tanaka, Y., Nishimura, A., 2007. Seasonal and depth variations in molecular and isotopic alkenone

composition of sinking particles from the western North Pacific. Deep Sea Research Part I: Oceanographic Research Papers 54, 1571–1592.

Yang, Y., Gao, C., Dang, X., Ruan, X., Lü, X., Xie, S., Li, X., Yao, Y., Yang, H., 2018. Assessing hydroxylated isoprenoid GDGTs as a paleothermometer for the tropical South China Sea. Organic Geochemistry 115, 156–165.

Yang, Y., Wang, C., Zhang, H., Huang, J., Xie, S., 2016. Influence of extraction methods on the distribution pattern and concentration of fatty acids and hydroxy fatty acids in soil samples: Acid digestion versus saponification. Geochemical Journal 50, 439–443.

Yao, J., Xiao, L., Gou, M., Li, C., Lian, E., Yang, S., 2018. Pacific decadal oscillation impact on East China precipitation and its imprint in new geological documents. Science China Earth Sciences 61, 473–482.

Yao, P., Yu, Z., Bianchi, T.S., Guo, Z., Zhao, M., Knappy, C.S., Keely, B.J., Zhao, B., Zhang, T., Pan, H., 2015. A multiproxy analysis of sedimentary organic carbon in the Changjiang Estuary and adjacent shelf. Journal of Geophysical Research: Biogeosciences 120, 1407–1429.

Zelles, L., Rackwitz, R., Bai, Q.Y., Beck, T., Beese, F., 1995. Discrimination of microbial diversity by fatty acid profiles of phospholipids and lipopolysaccharides in differently cultivated soils. Plant Soil 170, 115–122.

Zhang, Y.G., Zhang, C.L., Liu, X.-L., Li, L., Hinrichs, K.-U., Noakes, J.E., 2011. Methane Index: a tetraether archaeal lipid biomarker indicator for detecting the instability of marine gas hydrates. Earth and Planetary Science Letters 307, 525–534.

Figure Captions

Fig. 1. Location of surface sediment sampling sites in the North Pacific, including the South China Sea, the East China Sea, the Yellow Sea, the Bohai Sea, the Japan/East Sea, the Okhotsk Sea, and the Bering Sea. The black dots denote the surface sediments. The green star denotes the core sediment B3, the red triangle denotes the core sediment PN-2 and the blue squares denote core sediments DZ28 and DZ41 from East China Sea.

Fig. 2. Profile of excess ^{210}Pb ($^{210}Pb_{ex}$) for core B3. Accumulation rates were determined using best-fit linear methods to the slope of the line for the top 15 cm.

Fig. 3. Examples showing typical distributions of 3-OH-FAs from South China Sea, Yellow Sea and Bering Sea.

Fig. 4. (A) PCA biplot of 3-OH-FAs distributions in soils and marine sediments. The first principal component (PC1) explains 44% of the variation and the second principal component (PC2) explains 27% of the variation. (B) RDA triplot based on 3-OH-FAs proxies in marine sediments. The RDA1 explains 32% variation and the RDA2 explains 13% of the variation.

Fig. 5. Cross-plots of 3-OH-FA distributions in marine sediments (this study) and soils from Mt. Shenongjia reported by Wang et al. (2016). (A and B) Plots highlighting the differential distributions of *anteiso* and *normal* C_{15} (C_{17}) 3-OH-FAs in marine sediments and soils. (C and D) Plots highlighting the differential distributions of summed *anteiso*

3-OH-FAs in marine sediments and soils. (E and F) Extracted ion chromatogram (*m*/*z* 175) showing example distributions of 3-OH-FAs in marine sediments and soils.

Fig. 6. Ternary plot showing the distribution of 3-OH-FAs from marine sediments in this study and soil samples reported by Wang et al. (2016, 2018) and Huguet et al. (2019). The blue ellipse shows the domain of marine sediment distributions and the orange ellipse shows the domain of terrestrial soil distributions.

Fig. 7. Cross-plots showing the relationship between 3-OH-FAs based pH proxies (A–D, Branching Ratio, Branched Index, RIN and RIAN, respectively) and sea surface pH (https://www.nodc.noaa.gov/OC5/woa18/woa18data.html).

Fig. 8. Cross-plots showing the relationship between soil 3-OH-FA based pH proxies and annual mean SST in marine surface sediments.

Fig. 9. Phylum composition of Gram-negative bacterial communities for three soil samples collected from Mt. Yujia and three marine surface sediments from different water depths from the South China Sea.

Fig. 10. (A) Cross-plot showing the relationship between RAN_{13} and annual mean SST in marine sediments. (B) Cross plot showing the relationship between RAN_{13} and TEX_{86}-derived temperatures in our dataset. (C and D) Cross plots showing the relationship between temperature proxies (RAN_{13}, TEX_{86}^{H} and TEX_{86}^{L}) and mean annual SSTs in (sub)tropical (> 25 °C) and (sub)polar oceans (< 6 °C).

Fig. 11. (A) Cross plots showing exponential relationship between RAN_{13} and mean annual SSTs, and (B) the residual values between RAN_{13} estimated and satellite SSTs.

Fig. 12. Temporal variations in (A) PDO index (Yao et al., 2018), (B) Mean annual SST anomalies from the 1950s to the present day for the ECS (Bao and Ren, 2014) and (C) Instrumental mean annual SST for core B3 (gridded from NOAA) since the 1950s. (D) RAN_{13}-based SST in core B3 calculated using the exponential equation. The dashed line shows the linear trend during the time period. (E) Mean annual SSTs derived from TEX_{86}^{H} in core B3 and PN-2 (data from Lü et al. (2014)). (F) MAAT derived from MBT/CBT from core DZ28 and DZ41 (Chen et al., 2018).

Tables

Table 1 Location, environmental parameters and 3-OH-FAs based proxies for marine surface sediments from the North Pacific Ocean.

Sample	Latitude (°N)	Longitude (°E)	Depth (m)	SST (°C)	Branching Ratio	Branched Index	RIAN	RIN	RAN_{13}	RAN_{15}	RAN_{17}
S14-19	12.14	110.60	2300	27.7	0.55	0.35	0.26	0.25	0.82	15.01	5.68
934-20	12.19	109.75	155	27.5	0.34	0.25	0.47	0.24	0.73	3.45	1.82
ZSQD180	16.09	117.31	3960	28.1	0.46	0.31	0.34	0.23	0.61	10.79	3.76
HS13	19.96	115.14	971	26.4	0.50	0.33	0.30	0.24	1.71	16.34	6.83
STD33	20.48	114.83	126	26.2	0.45	0.31	0.34	0.28	1.32	7.38	3.94
STD29	21.12	114.47	83	25.6	0.58	0.37	0.24	0.31	1.06	7.20	4.99
STD330	22.82	118.54	39	25.4	0.43	0.30	0.36	0.30	1.21	5.38	2.78
A13-6	28.85	123.03	66	21.3	0.69	0.41	0.16	0.40	1.88	9.54	7.33
A12-6	29.05	123.15	69	21.1	0.70	0.41	0.16	0.41	1.49	7.52	4.51
A11-6	29.25	123.22	68	20.9	0.61	0.38	0.22	0.35	2.20	12.71	5.47
A11-5	29.33	122.98	67	20.6	0.71	0.42	0.15	0.45	1.64	8.60	5.30
A6-1	31.05	122.06	7	18.7	0.66	0.40	0.18	0.44	1.48	6.40	2.38
B6	31.37	122.12	15	18.5	0.56	0.36	0.25	0.37	1.95	6.29	4.68
B5	31.37	121.97	14	18.5	0.59	0.37	0.23	0.42	1.55	5.70	3.03
H29	33.01	123.00	32	17.2	0.74	0.43	0.13	0.44	1.60	6.64	6.23
H25	34.00	123.59	71	16.7	0.76	0.43	0.12	0.41	1.60	9.74	6.83
H16	35.00	121.66	46	15.6	0.86	0.46	0.06	0.46	1.74	9.30	6.32
HS4	35.50	122.31	53	15.3	0.79	0.44	0.10	0.41	1.83	9.79	6.88
H04	36.00	121.99	43	15.0	0.79	0.44	0.10	0.46	2.08	8.44	5.09
B35	37.11	121.22	30	14.3	0.88	0.47	0.06	0.52	2.11	8.51	5.69
BS04	37.40	123.09	56	14.1	0.77	0.44	0.11	0.46	2.05	9.40	5.94
B13	37.89	122.06	60	13.8	0.81	0.45	0.09	0.45	2.55	12.14	6.37
B72	37.94	120.32	18	13.9	0.82	0.45	0.08	0.48	2.00	9.09	5.60

B27	37.95	121.99	43	13.7	0.89	0.47	0.05	0.56	2.31	8.89	6.69
B43	38.32	119.35	24	14.0	0.82	0.45	0.08	0.53	1.97	7.23	4.46
B49	38.95	118.98	20	13.9	0.80	0.44	0.10	0.48	1.95	8.62	4.96
B58	39.49	120.44	25	13.1	0.80	0.44	0.10	0.50	1.90	8.34	4.80
LV55-25-2	39.80	133.90	n.d.	13.6	0.70	0.41	0.15	0.35	2.95	13.55	6.66
LV53-20-2	40.13	133.97	1147	13.3	0.77	0.43	0.11	0.40	3.08	14.17	7.50
LV53-18-2	42.95	134.75	587	10.2	1.01	0.50	-0.01	0.58	3.93	10.73	7.04
LV55-44-2	47.52	145.16	524	5.8	1.20	0.54	-0.08	0.71	4.14	9.62	6.71
LV55-29-2	51.90	144.70	n.d.	4.5	0.96	0.49	0.02	0.58	4.62	9.00	6.81
LV55-12-2	53.33	152.30	730	4.6	1.23	0.55	-0.09	0.84	3.63	7.99	6.78
LV55-18-2	56.30	145.30	n.d.	4.2	0.95	0.49	0.02	0.59	4.69	10.12	6.00
14NB02	60.87	175.53	107	3.8	0.94	0.49	0.03	0.56	4.79	8.72	6.42
14NB03	60.94	173.86	81	1.3	0.82	0.45	0.09	0.47	5.99	4.67	4.26
BS01	61.11	177.28	119	4.0	1.10	0.52	-0.04	0.65	5.39	7.67	5.00
BS02	61.12	175.54	91	3.6	0.89	0.47	0.05	0.52	6.21	8.57	4.69
BS03	61.13	173.88	70	3.0	1.22	0.55	-0.09	0.68	7.05	8.57	5.72
NB04	61.20	171.56	57	2.6	1.27	0.56	-0.10	0.73	5.71	9.91	5.88
BS04	61.25	171.63	49	2.6	1.28	0.56	-0.11	0.71	5.58	7.28	5.29
BM07	62.50	167.38	30	2.4	1.21	0.55	-0.08	0.76	6.39	10.03	6.15
BM04	62.63	173.00	55	2.4	1.04	0.51	-0.02	0.60	6.98	10.22	5.04
BM05	62.88	170.88	36	2.1	0.92	0.48	0.04	0.59	7.09	7.50	5.78
BM01	63.46	172.49	49	2.0	0.82	0.45	0.08	0.52	6.01	3.11	2.21

n.d. means no data.

Table 2 (A) RDA results applied to the fractional abundance of 3-OH-FAs in the marine sediments. The sum of all canonical eigenvalues is 0.46 and the total variance is 1. Eigenvalue (λ) is the proportion of the scores. λ as % of the sum of all canonical eigenvalues is obtained by multiplying by 0.46 with the variation explained by the first two axes. (B) The results of the forward selection. "Explains %" means the proportion of explanatory variables at a significance level of $p < 0.05$.

RDA axis	λ	λ as % of total inertia	λ as cumulative % of total inertia	λ as % of sum of all canonical eigenvalues
A				
1	0.32	32	32	74.3
2	0.13	13	45	91.7
B				
Order	Explanatory variable	Explains %	F Statistic	*p* Value
1	**SST**	**30**	**10.3**	**0.002**
2	pH	5	1.8	0.17
3	Salinity	2.3	0.8	0.52
4	Nitrate	4.3	1.6	0.2
5	Phosphate	1.6	0.6	0.59
6	Silicate	2.1	0.7	0.5
7	Water depth	0.9	0.3	0.88

Competing interest statement

The authors declare no competing interests.

Highlights

- Distinctive distributions of 3-OH-FAs in marine surface sediments vs soils
- 16S rRNA analysis shows distinct bacterial populations in marine sediments
- We propose RAN_{13} as a new proxy for sea surface temperature reconstruction

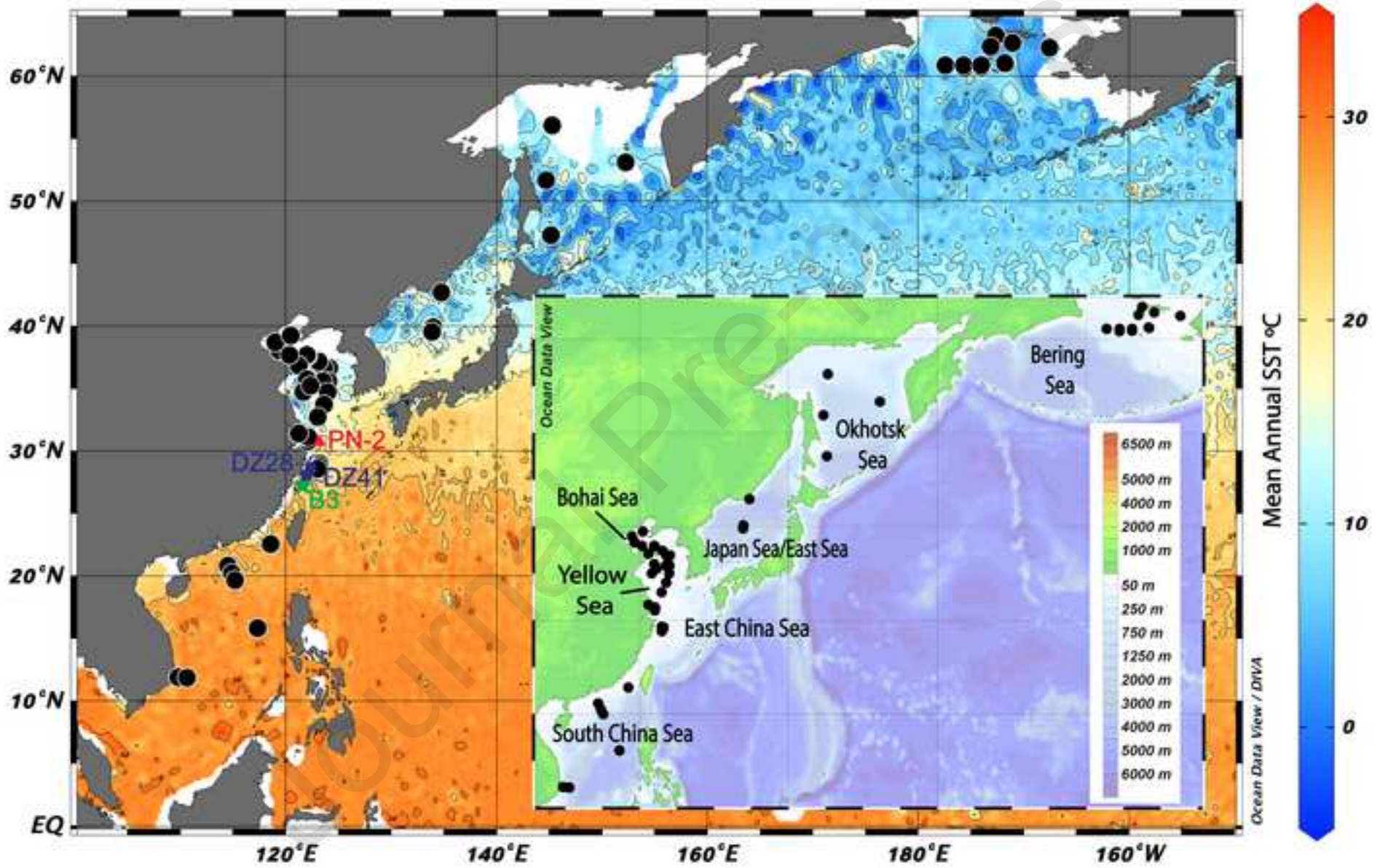
60°N
50°N
40°N
30°N
20°N
10°N
EQ
120°E
140°E
160°E
180°E
160°W
PN-2
DZ28
DZ41
B3
Ocean Data View
Bering Sea
Okhotsk Sea
Bohai Sea
Japan Sea/East Sea
Yellow Sea
East China Sea
South China Sea
6500 m
5000 m
4000 m
2000 m
1000 m
50 m
250 m
750 m
1250 m
2000 m
3000 m
4000 m
5000 m
6000 m
Mean Annual SST °C
30
20
10
0
Ocean Data View / DIVA